The *Journal of Cotton Science 18:85–93 (2014)*
http://journal.cotton.org, © The Cotton Foundation 2014

ENGINERING AND GINNING

Monitoring Cotton Root Rot Progression within a Growing Season Using Airborne Multispectral Imagery

Chenghai Yang*, Gary N. Odvody, Carlos J. Fernandez, Juan A. Landivar, Richard R. Minzenmayer, Robert L. Nichols, and J. Alex Thomasson

ABSTRACT

Cotton root rot, caused by the fungus *Phymatotrichopsis omnivora*, is a serious and destructive disease affecting cotton production in the southwestern United States. Accurate delineation of cotton root rot infections is important for cost-effective management of the disease. The objective of this study was to use airborne multispectral imagery for monitoring the progression of root rot infections within cotton fields during a growing season. A number of cotton fields near Edroy and San Angelo, Texas were selected for this study. Airborne multispectral digital imagery with blue, green, red and near-infrared bands was taken from these fields two to four times during the 2010 growing season. The imagery for two fields from each of the two locations was georeferenced and classified into two to twenty spectral classes using unsupervised classification techniques. The optimal number of spectral classes was determined based on the average transformed divergence for each classification and the spectral classes were then grouped into root rot-infected and non-infected zones. The infected areas within each field were determined for each imaging date and compared among the different dates. Both airborne imagery and ground observations showed that cotton root rot expanded in different patterns and at different rates over the growing season. Toward the end of the growing season, the percentage of root rot-infected areas increased to 13.2% and 26.8% in the two fields in Edroy, and to 37.8% and 50.6% in the two fields in San Angelo. The results from this study will be useful for the understanding of the progression of the disease and for the development of site-specific treatment plans for the disease.

Cotton root rot, caused by the soil-borne fungus *Phymatotrichopsis omnivora*, is one of the most destructive plant diseases occurring throughout the southwestern United States. The fungus is thermophilic and prevalent in alkaline soils. It has an extremely wide host range and has been reported as a pathogen for over 2000 dicotyledonous plants (Olsen, 2009). Cotton (*Gossypium hirsutum* L.) is an economically important crop throughout the southwestern U.S. and is highly susceptible to this disease. Infected plants wilt over a period of five to ten days and die with the leaves attached to the plants. The fungus kills plants typically in circular areas ranging from less than a square meter to several hectares in size (Smith et al., 1962). The symptoms usually begin during the period of rapid vegetative growth, are more visible during flowering and fruit development, and continue to increase through the growing season. The disease usually spreads over larger areas during years with adequate to excessive rainfall as moisture favors all aspects of the disease cycle. Plants infected earlier in the growing season will die before bearing fruit, whereas infection occurring at later plant growth stages will reduce cotton yield and lower lint quality (Ezekiel and Taubenhaus, 1934; Yang et al., 2005).

Cotton root rot has plagued the cotton industry for more than 100 years. Cultural practices such as deep ploughing, organic amendments, late planting, and rotation with monocotyledonous crops have been used to reduce the occurrence and severity of the disease (Fernandez, 2005; Rush and Lyda, 1984; Smith et al., 1962). Certain fumigants and fungicides applied to root rot-infected areas have provided reductions in the incidence of the disease, but such treatments have not always been effective nor economical for long-term control (Burnett,

C. Yang*, USDA-ARS Southern Plains Agricultural Research Center, 3103 F and B Road, College Station, TX 77845; G.N. Odvody, C.J. Fernandez, and J.A. Landivar, Texas AgriLife Research and Extension Center, 10345 State HWY 44, Corpus Christi, TX 78406; R.R. Minzemayer, Texas AgriLife Extension Service, 613 Hutchins Ave. Ste. 302, Ballinger, TX 76821; R.L. Nichols, Cotton Incorporated, 6399 Weston Parkway, Cary, NC 27513; and J.A. Thomasson, Texas A&M University, 201 Scoates Hall, College Station, TX 77843
*Corresponding author: chenghai.yang@ars.usda.gov

1970; Lyda et al., 1967; Lyda and Rush and Lyda, 1989; Whitson and Hine, 1986). Recently, a commercial formulation of flutriafol (TOPGUARD® - Cheminova, Inc., Wayne, NJ) has been found to effectively control cotton root rot (Isakeit et al., 2009, 2010, 2012). More experiments are being conducted to determine optimal effective rates, application methods and timing on the use of this fungicide for both irrigated and dryland cotton fields. Since the disease infects only portions of the field, it will be more economical and environmentally friendly to treat only the infected areas. Therefore, it is necessary to define the infected areas and understand the seasonal spread of the disease within the field so that variable rate technology can be used for the control of the disease.

Remote sensing is perhaps the only practical means for effectively mapping this disease because of large numbers of infected areas and their irregular shapes within cotton fields. In fact, this technology has long been used to document the distribution of cotton root rot damage with cotton fields (Nixon et al., 1975; 1987; Taubenhaus et al., 1929). More recently, Yang et al. (2005) integrated airborne multispectral digital imagery with global positioning system (GPS) and image classification techniques to accurately detect and map root rot infections within cotton fields in south Texas for site-specific management. Yang et al. (2010) compared airborne multispectral and hyperspectral imagery for detecting and mapping root rot areas in cotton fields. Image classification and accuracy assessment of the root rot maps showed that both types of imagery accurately identified root rot-infected areas and can be used for assessing root rot infection within cotton fields.

In previous studies, remote sensing imagery has been successfully used to map cotton root rot infections near the end of the growing season when cotton root rot is fully pronounced for the season. However, little work has been done to monitor the progression of the disease over the growing season. This information is important for the understanding of the initiation and subsequent development and progression of the disease. It can also be used to formulate site-specific strategies for the control of the disease. With the recent temporary authorization for use of the fungicide flutriafol to control cotton root rot in Texas by means of a section 18 of the Federal Insecticide, Fungicide, and Rodenticide Act (FIFRA), more research is needed to study the progression of this disease under fungicide-treated and untreated conditions and the efficacy of different treatments using remote sensing and other emerging technologies in a multidisciplinary approach. Therefore, the objective of this study was to use airborne multispectral imagery for monitoring the progression of cotton root rot infections in cotton fields within a growing season.

MATERIALS AND METHODS

Study Sites. This study was conducted at two cotton-growing areas in Texas, one in Edroy and the other in San Angelo. Approximately a dozen irrigated and dryland fields were selected from each area for aerial imaging. Two representative fields from each area are depicted in this article. These fields had a history of cotton root rot. Table 1 shows the geographical location, field size and irrigation type for each of the four fields at the two study sites.

Airborne Multispectral Image Acquisition. Airborne multispectral imagery was acquired using a four-band imaging system described by Yang (2012). The system consists of four high-resolution charge-coupled device (CCD) digital cameras and a ruggedized PC equipped with a frame grabber and image acquisition software. The cameras are sensitive in the 400 to 1000 nm spectral range and provide 2048 × 2048 active pixels with 12-bit data depth. A 24-mm lens is attached to each camera, resulting in an imaging size of 0.63 times the flight altitude. The four cameras are equipped with blue (430-470 nm), green (530-570 nm), red (630-670 nm), and near-infrared (NIR) (810-850 nm) band-

Table 1. Geographical locations, field size and irrigation type for four cotton fields at two study sites.

Sites	Field	Latitude	Longitude	Area (ha)	Irrigation type
Edroy	1	28°07′39″N	97°41′44″W	92.5	Center pivot
Edroy	2	27°59′53″N	97°42′49″W	86.1	Dryland
San Angelo	1	31°26′31″N	100°22′16″W	11.3	Drip
San Angelo	2	31°24′12″N	100°08′22″W	25.5	Center pivot

pass interference filters, respectively. They are arranged in a quad configuration and attached to adjustable mounts that facilitate aligning the cameras horizontally, vertically, and rotationally. The image acquisition software allows the synchronized black-and-white band images from the cameras to be viewed on the computer monitor in any one of the four modes: a quad (four bands at a time), one band image at a time, a normal color composite, or a color-infrared (CIR) composite. The band images are refreshed continuously to allow the operator to selectively save images with desired areas of interest. The selected four-band composite image is saved as a Tiff file and consecutive images can be saved at one-second intervals.

Images were acquired at altitudes of approximately 2740 m above ground level between 1200 and 1500h local time under sunny conditions on four different dates (July 12, 30, August 11, and 23, 2010) in Edroy and three different dates (July 25, August 23 and September 27, 2010) in San Angelo. A Cessna 206 aircraft was used to acquire the imagery. The imagery had ground pixel sizes of approximately 0.85 m based on the pixel array (2048 x 2048) and flight height.

Image Alignment and Rectification. An image-to-image registration procedure based on the first-order polynomial transformation model was used to align the four individual band images in each composite image. The red band image was used as the reference and the other three band images in each composite were registered to it to correct the misalignments among the four band images. One different transformation model was required for each of the three bands. To determine the transformation model coefficients, 8-12 evenly-distributed reference points were identified from each image. The root mean square (RMS) errors among the bands were generally from half a pixel to less than two pixels for the images.

The registered images were then georeferenced or rectified to the Universal Transverse Mercator (UTM), World Geodetic Survey 1984 (WGS-84), Zone 14, coordinate system based on a set of ground control points (12-15) around each field located with a Trimble GPS Pathfinder ProXRT receiver (Trimble Navigation Limited, Sunnyvale, California). The OmniSTAR XP satellite-based differential correction service (OmniSTAR, Inc., Houston, Texas) was used with the GPS receiver to achieve real-time 20-cm accuracy. The RMS errors for rectifying the images using first-order transformation were approximately two meters. All images were resampled to one-meter resolution using the nearest neighborhood technique. All procedures for image registration and rectification were performed using ERDAS Imagine (ERDAS Inc., Norcross, Georgia).

Image Classification. The rectified, four-band multispectral images were classified into two to twenty spectral classes using ISODATA (Iterative Self-Organizing Data Analysis) unsupervised classification (Campbell, 2002; ERDAS, 2010). The unsupervised method uses minimum spectral distance to group each pixel to a class. The process began with arbitrary class means from the image statistics based on the number of classes specified. It repeatedly performed a classification and recalculated new class statistics, which were used for the next iteration. The process continued until the number of iterations reached 200 or the convergence threshold reached 1.00. In all the classifications, the convergence threshold was met before the maximum number of iterations was reached.

To evaluate the separability of the spectral classes for each classification map, the average transformed divergence was calculated among all possible pairs of classes for each classification based on the four bands. The transformed divergence measures the statistical distance between any two spectral signatures (classes) and is calculated using the mean band vectors and band covariance matrices of the two signatures (ERDAS, 2010; Jensen, 1996). The spectral classes in each classification map were then grouped into root rot-infected and non-infected zones by comparing with the original image and based on ground observations. The root rot-infected areas and non-infected areas were estimated from the best two-zone classification maps.

Root rot-infected areas can be accurately differentiated from non-infected areas if there are no other major stressors present that produce similar plant symptoms to those of root rot (Yang et al., 2005 and 2010). Field observations confirmed that cotton root rot was the dominant stressor and there was a minimal amount of interference from other biotic and abiotic factors in these cotton fields. Therefore, the two-zone classification maps using the unsupervised classification and regrouping procedures were accurate and reliable. Nevertheless, care was taken to ensure infected areas were correctly identified by visually comparing each classification map with its original CIR and normal color images.

RESULTS AND DISCUSSION

Figure 1 shows CIR images acquired on the four dates for field 1 in Edroy, TX. On the CIR images, healthy plants showed a reddish-magenta tone, while infected plants had a greenish or cyanish color. The root rot-infected areas could be easily separated from the non-infected areas on the CIR images. Excessive rainfall in the Edroy area created very favorable conditions for the development of root rot during the early part of the 2010 growing season, but the rainfall pattern and associated cloudy weather made it difficult to take timely and complete images for the study fields. Due to ample soil moisture, it was not necessary to irrigate the field, which had two center pivots. Although all the fields were confirmed to have the onset of cotton root rot on 2 June, the first set of images was not captured until 12 July. By this date, the cotton root rot had expanded substantially within each field. The July 30 image revealed that root rot continued to expand from the infected areas shown on the 12 July image. In field 1, the fungus seemed to expand predominantly in circular patterns, though some infected areas had irregular shapes. Moreover, the fungus might have either expanded outward from the center of an infected area or spread inward from the outside perimeter of an infected area toward the center. By August 11, the lower portion of the field was defoliated to prepare for harvest. There had been no substantial increase in root rot from the previous date. By August 23, the field had already been harvested, but root rot-infected areas still can be clearly seen in the image. The only difference was that most of the infected areas were taken over by weeds, giving these areas a reddish color on the CIR image.

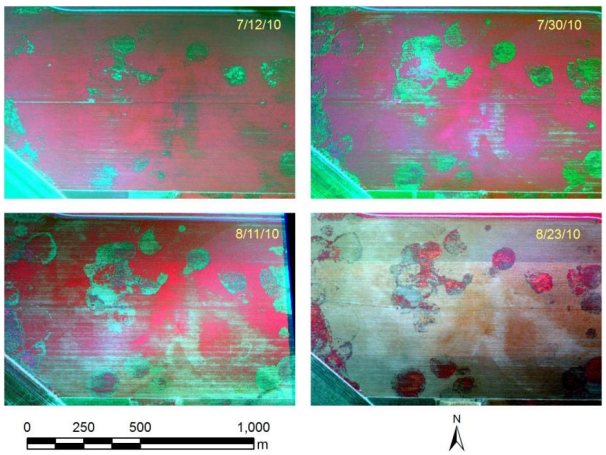

Figure 1. Airborne CIR images acquired on four dates during the 2010 growing season from a 92.5-ha cotton field (field 1) infected with cotton root rot in Edroy, TX.

Table 2 gives the average transformed divergence values among all possible pairs of the spectral classes when each image was classified into two- to twenty-class unsupervised classification maps for the two fields in Edroy, TX on 12 and 30 July 2010. The average transformed divergence values ranged from 1623 to 1945 among the 76 different classification maps for the two fields on the two dates. For example, a ten-class classification map has 45 possible pairs of classes. The average transformed divergence for the ten-class classification map was the average of the 45 divergence values calculated for all the possible pairs. The transformed divergence value ranges from 0 to 2000. If the calculated divergence is equal to 2000, then the signatures can be said to be completely separable in the bands being studied. A calculated divergence of zero means that the signatures are inseparable. As a general rule, if the result is greater than 1900, then the classes can be separated; between 1700 and 1900, the separation is good; below 1700, the separation is poor (Jensen, 1996).

Divergence values generally increased with the number of classes, but there were a few exceptions. For example, the transformed divergence value was 1843 for the two-class classification on 12 July 2010 for Field 2 and that value is higher than the value 1778 for the three-class classification or the value 1830 for the four-class classification for the same field on the same date. Although increasing the number of classes tends to increase the separability among the classes, it will also increase the computing time. When the transformed divergence value reaches 1900, the classification is considered excellent. According to this guideline, the optimal number of classes was nine for 12 July and 16 for 30 July for Field 1 and ten for 12 July and 14 for 30 July for Field 2 in the Edroy area in 2010.

Figures 2 and 3 show the multi-class unsupervised classification maps and the merged two-zone maps on the two dates for fields 1 and 2, respectively. On the multi-class unsupervised classification maps, pinkish and reddish colors represent root rot areas, while the blue, cyan, green, yellow, and orange and other colors represent the areas that were not infected with root rot, but exhibited differences in growth. The merged two-zone classification maps were formed by grouping the classes into root rot-infected areas (red) and non-infected areas (green). A visual comparison of the classification maps and their respective CIR images indicated that the two-zone classification maps effectively identified apparent root rot areas within the fields.

Table 2. Average transformed divergence among all possible pairs of the spectral classes (signatures) when each image was classified into two- to twenty-class unsupervised classification maps for two fields in Edroy, TX on two dates in 2010. The scale of the divergence values range from 0 to 2000. A higher value indicates a better separation among the classes. All the values greater than or equal to 1900 are bolded.

No. of Spectral Classes	Field 1		Field 2	
	7/12/2010	7/30/2010	7/12/2010	7/30/2010
2	1623	1718	1843	1852
3	1723	1744	1778	1851
4	1841	1788	1830	1820
5	1872	1808	1853	1843
6	1878	1814	1863	1859
7	1895	1824	1874	1862
8	1895	1828	1886	1877
9	**1907**	1841	1896	1889
10	**1913**	1851	**1903**	1898
11	**1905**	1860	**1903**	1898
12	**1910**	1872	**1912**	1899
13	**1911**	1885	**1917**	1899
14	**1918**	1891	**1923**	**1906**
15	**1915**	1896	**1927**	**1909**
16	**1919**	**1903**	**1928**	**1915**
17	**1924**	**1908**	**1936**	**1917**
18	**1928**	**1914**	**1942**	**1921**
19	**1929**	**1918**	**1944**	**1925**
20	**1932**	**1922**	**1945**	**1927**

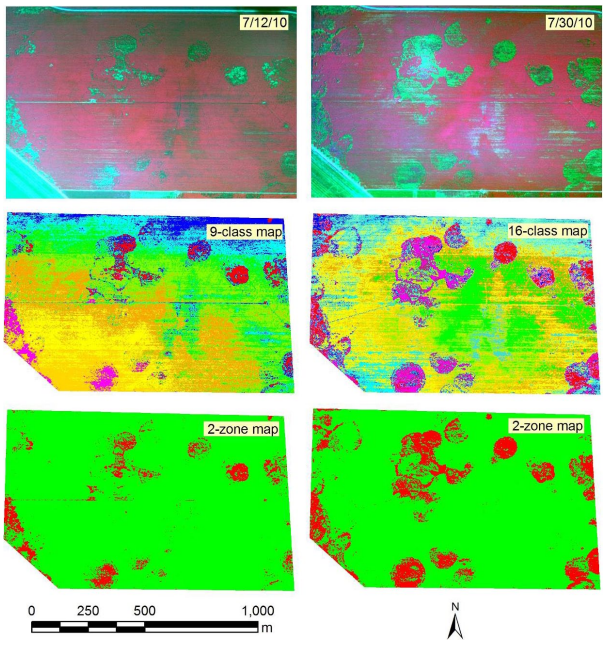

Figure 2. CIR images, 9-class unsupervised classification map for 12 July and 16-class unsupervised classification map for 30 July, and merged 2-zone maps for the two respective dates for a 92.5-ha cotton field (field 1) infected with cotton root rot in Edroy, TX. In the two-zone maps, red represents root rot-infected areas and green depicts non-infected areas.

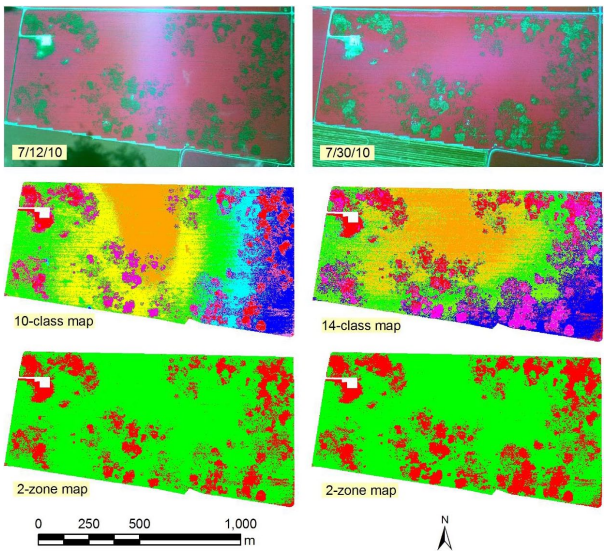

Figure 3. CIR images, 10-class unsupervised classification map for 12 July and 14-class unsupervised classification map for 30 July, and merged 2-zone maps for the two respective dates for an 86.1-ha cotton field (field 2) infected with cotton root rot in Edroy, TX. In the two-zone maps, red represents root rot-infected areas and green depicts non-infected areas.

Table 3 gives the optimal number of spectral classes and root rot-infected areas estimated from the two-zone maps for fields 1 and 2 in Edroy, TX on the two dates in 2010. The estimated percent root rot areas in field 1 increased from 5.4% on 12 July to 13.2% on 30 July. In comparison, the estimated percent root rot areas in field 2 increased from 21.6% on 12 July to 26.8% on 30 July.

Table 4 gives the average transformed divergence values among all possible pairs of the spectral classes when each image was classified into two- to twenty-class unsupervised classification maps for the two fields in San Angelo, TX on 23 August and 27 September 2010. The transformed divergence values ranged from 1721 to 1921 among the 76 different classification maps for the two fields on the two dates. Similarly, divergence values generally increased with the number of classes. The optimal number of classes was 18 for 23 August and 16 for 27 September for field 1 and 14 for 23 August and 17 for 27 September for field 2 in San Angelo, TX in 2010. The transformed divergence values for the four respective classifications were 1904, 1901, 1900, and 1904.

The top portions of Figures 4 and 5 show the CIR images acquired on the three dates for fields 1 and 2, respectively, in San Angelo, TX. By 25 July, root rot symptoms were noted in both fields. By 23 August, the fungus had spread across the fields. Unlike field 1 in Edroy where the fungus spread dominantly in circular patterns, the fungus expanded in irregular patterns in these fields. By 27 September, shortly before harvest, root rot had expanded to cover significant portions of the fields.

Table 3. Optimal number of spectral classes and root rot-infected areas for two fields in Edroy, TX on two dates in 2010.

	Field 1		Field 2	
	7/12/2010	7/30/2010	7/12/2010	7/30/2010
No. of Classes	**9**	**16**	**10**	**14**
Total Area (ha)	**92.5**	**92.5**	**86.1**	**86.1**
Infected Area (ha)	**5**	**12.2**	**18.6**	**23.1**
Infected Area (%)	**5.4**	**13.2**	**21.6**	**26.8**

Table 4. Average transformed divergence among all possible pairs of the spectral classes (signatures) when each image was classified into two- to twenty-class unsupervised classification maps for two fields in San Angelo, TX on two dates in 2010. The scale of the divergence values range from 0 to 2000. A higher value indicates a better separation among the classes. All the values greater than or equal to 1900 are bolded.

No. of Spectral Classes	Field 1		Field 2	
	8/23/2010	9/27/2010	8/23/2010	9/27/2010
2	1721	1844	1640	1793
3	1734	1665	1704	1744
4	1779	1738	1752	1777
5	1757	1797	1803	1778
6	1790	1843	1824	1815
7	1792	1867	1810	1810
8	1808	1846	1841	1820
9	1832	1851	1860	1838
10	1839	1865	1864	1851
11	1857	1865	1877	1857
12	1866	1878	1889	1869
13	1874	1887	1892	1877
14	1882	1892	**1900**	1884
15	1890	1896	1892	1892
16	1896	**1901**	**1908**	1898
17	1898	**1907**	**1911**	**1904**
18	**1904**	**1913**	**1908**	**1908**
19	**1908**	**1914**	**1916**	**1910**
20	**1912**	**1920**	**1921**	**1915**

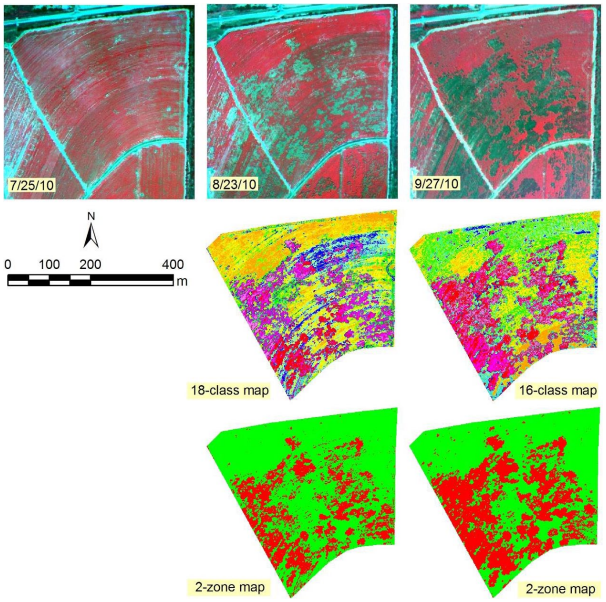

Figure 4. CIR images, 18-class unsupervised classification map for 23 August and 16-class unsupervised classification map for 27 September, and merged 2-zone maps for the two respective dates for an 11.3-ha cotton field (field 1) infected with cotton root rot in San Angelo, TX. In the two-zone maps, red represents root rot-infected areas and green depicts non-infected areas.

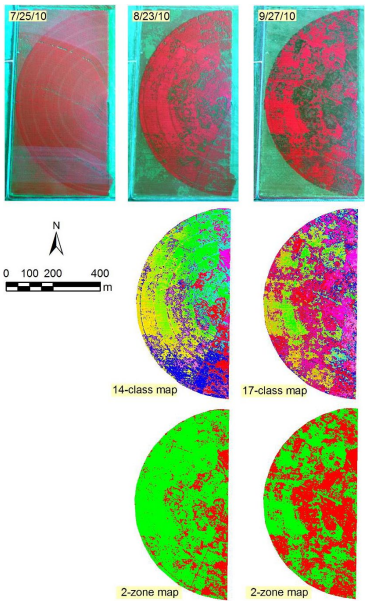

Figure 5. CIR images, 14-class unsupervised classification map for 23 August and 17-class unsupervised classification map for 27 September, and merged 2-zone classification maps for the two respective dates for a 25.5-ha cotton field (field 2) infected with cotton root rot in San Angelo, TX. In the two-zone maps, red represents root rot-infected areas and green depicts non-infected areas.

The middle and lower portions of Figures 4 and 5 show the optimal unsupervised classification maps along with the respective merged two-zone maps on 23 August and 27 September 2010 for fields 1 and 2, respectively. A visual comparison of the classification maps and their respective CIR images indicated that the two-zone classification maps accurately identified root rot areas within the fields. Yang et al. (2005 and 2010) performed accuracy assessments on unsupervised classification maps derived from both multispectral and hyperspectral imagery for four different cotton fields. Their results indicate that overall accuracy of the two-zone classification maps for the four fields was from 95% to 98% and the producer's and user's accuracies for the images were from 94 to 100%.

Table 5 gives the optimal number of spectral classes and root rot-infected areas estimated from the two-zone maps for fields 1 and 2 in San Angelo, TX on the two dates in 2010. The estimated percent root rot areas increased from 27.0% on 23 August to 37.8% on 27 September in field 1 and from 21.4% on 23 August to 50.6% on 27 September in field 2. Clearly, root rot-infected areas in field 2 more than doubled during the 35-day period toward the end of the growing season.

SUMMARY

Airborne multispectral imagery taken from four cotton fields in two cotton growing areas in Texas on multiple dates within the 2010 growing season was used to monitor the progression of cotton root

Table 5. Optimal number of spectral classes and infected root rot areas for two fields in San Angelo, TX on two dates in 2010.

	Field 1		Field 2	
	8/23/2010	9/27/2010	8/23/2010	9/27/2010
No. of Classes	18	16	14	17
Total Area (ha)	11.3	11.3	25.5	25.5
Infected Area (ha)	3.1	4.3	5.5	12.9
Infected Area (%)	27	37.8	21.4	50.6

rot. Each image was classified into two to twenty spectral classes using unsupervised classification techniques. The optimal number of spectral classes was determined based on the average transformed divergence for each classification map and the spectral classes were then grouped into root rot-infected and non-infected zones. Both airborne imagery and ground observations showed that cotton root rot expanded in different patterns and at different rates over the growing season. By the end of the season, the percentage of root rot-infected areas increased to 13.2% and 26.8% in the two fields in Edroy, and to 37.8% and 50.6% in the two fields in San Angelo.

The results from this study demonstrate that airborne multispectral imagery in conjunction with unsupervised classification is an effective tool for monitoring and mapping cotton root rot infections within cotton fields during the growing season. These results will be useful for the understanding of the progression of the disease and for the development of site-specific treatment plans for the disease. It should be noted that root rot was the dominant stressor in the study fields at both locations, even though other minor biotic and abiotic stressors may have been present. However, because the fungus kills cotton plants so quickly, it has a very unique signature on the airborne imagery compared with other stressors such as nutrient deficiencies and minor insect damage. Therefore, other factors have minimal effects on the identification of root rot-infected areas within the fields. The cause of differences observed in multispectral images must be confirmed by trained field personnel because multiple stressors that can cause plant wilting or death as root rot does will affect the accuracy of the mapping results for cotton root rot.

Although adverse weather conditions delayed the start of image acquisition in the Edroy area, the temporal images obtained from the fields successfully monitored the progression and documented the extent of the disease within each field from shortly after the initiation of the disease to the end of the growing season. The images and classification maps from this study will be useful for studies of the interactions among soil properties and other biological, crop growth, and environmental factors associated with cotton root rot. For long-term effective and economical management of this disease, it is necessary to not only understand the within-season progression patterns, but also to monitor the consistency and variation of the spatial patterns from year to year.

ACKNOWLEDGEMENT

This project was partly funded by Cotton Incorporated, Cary, NC. The authors wish to thank Michael Ohlinger of Sterling Air Service at Weslaco, TX and Fred Gomez of USDA-ARS at College Station, TX for taking the multispectral imagery for this study and Jim Forward of U.S. Fish and Wildlife Service at Alamo, TX for assistance in image registration.

DISCLAIMER

Mention of trade names or commercial products in this article is solely for the purpose of providing specific information and does not imply recommendation or endorsement by the U.S. Department of Agriculture. USDA is an equal opportunity provider and employer.

REFERENCES

Campbell, J.B. 2002. Introduction to Remote Sensing, 3rd ed. The Guilford Press, NY.

ERDAS. 2010. ERDAS Field Guide. ERDAS, Inc., Norcross, GA.

Ezekiel, W.N., and J.J. Taubenhaus. 1934. Cotton crop losses from phymatotrichum root rot. J. Agric. Res. 49(9):843-858.

Fernandez, C.J., C. Yang, and J.H. Everitt. 2005. Late-planting decreased cotton root rot infestations in irrigated fields. Proc. Beltwide Cotton Conf., New Orleans, LA 4-7 Jan. 2005. Natl. Cotton Counc. Am., Memphis, TN, pp. 197-202.

Isakeit, T., R.R. Minzenmayer, and C.G. Sansone. 2009. Flutriafol control of cotton root rot caused by Phymatotrichopsis omnivora. Proc. Beltwide Cotton Conf., San Antonio, TX 5-8 Jan. 2009. Natl. Cotton Counc. Am., Memphis, TN, pp. 130-133.

Isakeit, T., R.R. Minzenmayer, A. Abrameit, G. Moore, and J.D. Scasta. 2010. Control of phymatotrichopsis root rot of cotton with flutriafol. Proc. Beltwide Cotton Conf., New Orleans, LA 4-7 Jan. 2010, 200-203. Natl. Cotton Counc. Am., Memphis, TN.

Isakeit, T., R.R. Minzenmayer, D.R. Drake, G.D. Morgan, D.A. Mott, D.D. Fromme, W.L. Multer, M. Jungman, A. Abrameit. 2012. Fungicide management of cotton root rot (phymatotrichopsis omnivora): 2011 results. Proc. Beltwide Cotton Conf., Orlando, FL, Jan. 3-6, 2012, 235-238. Natl. Cotton Counc. Am., Memphis, TN.

Jensen, J.R. 1996. Introductory Digital Image Processing: A Remote Sensing Perspective, 2nd ed. Prentice-Hall, Englewood Cliffs, NJ.

Lyda, S.D., and E. Burnett. 1970. Influence of benzimidazole fungicides on Phymatotrichum omnivorum and Phymatotrichum root rot of cotton. Phytopathology 60:726-728.

Lyda, S.D., G.D. Robison, and H.W. Lembright. 1967. Soil fumigation control of phymatotrichum root rot in Nevada. Plant Disease Reporter 51(5):331-333.

Nixon, P.R., S.D. Lyda, M.D. Heilman, and R.L. Bowen. 1975. Incidence and control of cotton root rot observed with color infrared photography. Pub. No. MP1241. Texas A&M Agricultural Experiment Station, College Station, TX.

Nixon, P.R., D.E. Escobar, and R.L. Bowen. 1987. A multispectral false-color video imaging system for remote sensing applications. Proc. 11th Biennial Workshop on Color Aerial Photography and Videography in the Plant Sciences and Related Fields, 295-305, 340. American Society for Photogrammetry and Remote Sensing, Bethesda, MD.

Olsen, M.W. 2009. Cotton (Texas) Root Rot. Pub. No. AZ1150. The University of Arizona Cooperative Extension, Tucson, AZ.

Rush, C.M. and T.J. Gerik. 1989. Relationship between postharvest management of grain sorghum and Phymatotrichum root rot in the subsequent cotton crop. Plant Disease 73(4):304-305.

Rush, C.M., and S.D. Lyda. 1984. Evaluation of deep-chiseled anhydrous ammonia as a control for phymatotrichum root rot of cotton. Plant Disease 68:291-293.

Smith, H.E., F.C. Elliot, and L.S. Bird. 1962. Root rot losses of cotton can be reduced. Pub. No. MP361. Texas A&M Agricultural Extension Service, College Station, TX.

Taubenhaus, J.J., W.N. Ezekiel, and C.B. Neblette. 1929. Airplane photography in the study of cotton root rot. Phytopathology 19:1025-1029.

Whitson, R.S., and R.B. Hine. 1986. Activity of propiconazole and other sterol-inhibiting fungicides against Phymatotrichum omnivorum. Plant Disease 70:130-133.

Yang, C. 2012. A high resolution airborne four-camera imaging system for agricultural applications. Computers and Electronics in Agriculture 88:13-24.

Yang, C., C.J. Fernandez, and J.H. Everitt. 2005. Mapping Phymatotrichum root rot of cotton using airborne three-band digital imagery. Transactions of the ASAE 48(4):1619-1626.

Yang, C., C.J. Fernandez, and J.H. Everitt. 2010. Comparison of airborne multispectral and hyperspectral imagery for mapping cotton root rot. Biosystems Engineering 107:131-139.